Contents lists available at http://qu.edu.iq

Al-Qadisiyah Journal for Engineering Sciences

Journal homepage: http://qu.edu.iq/journaleng/index.php/JQES

Semisolid state sintering behavior of aluminum-stainless steel 316L-nickel composite materials in powder metallurgy

Ali A. Oudah*, Mahmoud A. Hassan, and Nabeel Almuramady

Department of Mechanical Engineering, College of Engineering, University of Al-Qadisiyah, Al Diwaniyah, Iraq

ARTICLE INFO

Article history:
Received 01 July 2022
Received in revised form 07 August 2022
Accepted 18 September 2022

Keywords:
Alu. Alloy 316L
Sintering
Powder
Milling

ABSTRACT

Powder metallurgy (PM) is a primarily used because of its relatively close capability and cost-achievement ratio. The automotive industry is considered a major market for the powder metallurgy industry, as it necessitates products having superior mechanical or part of the implementation on a global level. PM technology is undergoing considerable changes in manufacturing and materials research as automobile technologies transitions beyond classic gasoline - powered vehicles to new energy vehicles. Changes in automobile technologies has created both obstacles and opportunities for PM, as outlined in this article. The mechanical properties of FGM (Al-Ni-steel) sample were investigated using hardness and tensile tests. Transmission electron microscopy (SEM) and X-ray Diffraction Instrument analysis were also used to analyze the microstructure of FGMs in detail by using Xpert analytical program. Tensile specimens were made from sintered cylindrical rods with a length of 150 mm size with diameter of 10 mm. Tensile samples with the circular section size of 1cm and a length of 3 cm are machined according to ASTM E-8M. Homogeneous beams comprising varied weight fractions of Al (aluminum), Ni (nickel), and 316 steel are fabricated and tensile tests are performed to estimate the elastic modulus of horizontally layered functionally graded (FGMs) rods. Each homogenous layer's density is also calculated experimentally.

1. Introduction

Materials are constantly being produced, ranging from iron to pure metals to composite materials that are currently in use**. Fig. 1** [1] depicts the evolution of materials from the Bronze Age to the current day and into the future. Pure metals have a relatively restricted use since real-world applications may demand properties that a single metal cannot give. Alloys are often stronger and more versatile than pure metals. The earliest alloy produced in 4000 BC was bronze, which is a copper-tin alloy (Bronze age). Since then, many metal and non-metal mixes have been explored to combine the strengths of numerous materials according to functional requirements. The volume or weight percentage, configuration, and geometry of changes in phase distribution can all be converted. The change in volume fraction might occur in any direction or immediately over the full thickness of the component (such as the coordinates of the plate or beam). Because of its modest expansion capacity, the ceramic area has high heat

* *Corresponding author.*
E-mail address: mark6ge@gmai.com(Ali A.Oudah)

https://doi.org/10.30772/qjes.v15i3.838

Nomenclature

XRD	X-ray direction
fesem	scanning electron microscopy
XRF	X-ray fluorescence
FWHM	Full width at half maximum

Greek symbols

K	Scherrer constant
2Θ	the angle between transmitted beam and reflected beam.
λ	the X-ray wavelength
B	the line boarding at FWHM in radian.

Subscripts

D	is the crystallite size
Hkl	the assignment of the Miller Indices

resistance. Ductile metal components can withstand stress caused by rapid temperature fluctuations in a short period of time[2],. The volume or weight percentage, configuration, and geometry of changes in phase distribution can all be converted. The change in volume fraction might occur in any direction or immediately over the full thickness of the component (such as the coordinates of the plate or beam). Because of its modest expansion capacity, the ceramic area has high heat resistance. Ductile metal components can withstand stress caused by rapid temperature fluctuations in a short period of time [3], [4]. Composite materials provide a higher strength-to-stiffness ratio, better fatigue, wear, and corrosion resistance, and higher dependability than pure or alloyed metals.

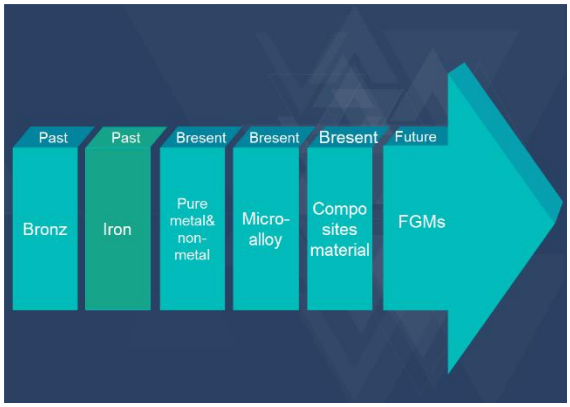

Figure 1. From bronze to FGMs, material progress has been continuous

Despite these benefits, composite materials have an abrupt shift of characteristics at the interface, which can lead to components failure by (delamination) [5]under excessive operating conditions in which delamination is a failure mode in which a material cracks into layers. Delamination may occur in a number of materials, such as multilayer composites [6] and concrete. Layer separation may cause failure in metals such as steel rolling[7],[8]. and polyester and metals created by 3-dimensional printing,[3]. Delamination of coating materials including such paints and films from of the upon is also a possibility. The adhesion between layers in laminated composites frequently breaks first, leading layers to split. [4] In Glass(fiber) Reinforced Plastic (GRP), for example, plates of strong reinforcing (such as fiberglass) are linked together with a considerably weaker matrix material (e.g., epoxy). In particular, loads applied orthogonally to the high potency layers, and shear stresses could indeed cause the polymer structure to fracture or the reinforcement materials to split from the composite material. The purpose of this work is to discuss functionally gradient materials (FGMs), their kinds, and manufacturing processes.

FGMs are also studied using solid free form fabrication (SFF) methods. FGM is a revolutionary hybrid material that tailors material properties to individual application requirements, revolutionizing materials research. Nevertheless, there are still roadblocks in the way of achieving this objective[9]. Other challenges include a lack of data obtained, as well as technology such as mass production to properly leverage this approach., and so on, in addition to the primary cost issue. Many studies on successful manufacturing methods for FGM are already underway; nevertheless, there are still a number of challenges that need to be addressed with these emerging technologies[10]. More research is required to build a suitable database, which will include detailed characterization of FGMs and the development of prediction models for proper process control, allowing for the creation of more effective FGMs. An effective feedback system is essential in fully formed automated manufacturing processes; hence, for total process control improvement, extensive research is required[11]. PM is very effective for FGMs manufacture; nevertheless, various challenges, including as size and shape limitations, powder cost (which is more than castings material), complexity in producing a continual gradient, & sintering defect, still need to be addressed[12].

2. Materials and methods

Nickel, Steel316L and aluminum powders were used as raw materials to make the FGMs in this section[13]. Because reason steel 316L was utilized, low carbon steel has a low melting point temperature. The matrix materials were as-atomized Al powders (99.8% purity) including an mean particle size of 18.3 m (CDH Company, India), Steel 316L powder samples with a mean particle size of 45 m (cangsha Easchem Co, China) were used as toughness reinforcements, and Nickel powder samples with a mean particle size of 9.922 m (Metco Company, Germany) were used as reinforcements. Expectantly improve the mechanical characteristic at dynamic load[14]. A hybrid FGM (AI-Ni-steel 316L) with varying volume and amount has been created. Powder metallurgy was used to create three different types of layered Al-Ni-Steel functionally graded materials in this study. Five layers consist of the FGMs samples., all the initial layer 2mm thickness is created by (%75. Ni,%25. Al) and all the fifth layer has a thickness of 2 mm. (%33.3 Ni, %33.3Al, %33.3 316L Steel). Each layer's ingredients are combined according to pre-determined weight ratios. For all concentrations, the mass of Ni, Al, and 316L Steel is shown in Table 1, that have been used in this study. The weight of the compounds is calculated by using specific density of the powder.

Milling could be done in strong shaker crushers, in which small quantities of about 10 to20 g have been milled at quite a period, mostly by alloy inspection, or in lesser planetary milling, in which large amounts of particles (approximately 200 g) could be shredded, or in attritors, where even larger quantities can be milled at once. Shaker crushers operate within about 1200 rev / min, radial mills at 150 to 600 rev/min, and powder at 100

to 200 rpm. Each layer's ingredients are blended according to predetermined weight ratios. MTI Ball Mall was used to keep the mixing duration consistent for all samples (30 minutes) [108]. 10 mm in length and diameter were used to create functionally graded material samples.

Table 1. illustrates the weight composition distribution of the first Al-Ni-316L Steel sample1 for FGM.

Layer number	%Ni	%Al	%Steel	Thickness layer(mm)	Compound weight(gm)
1	75	25	0	2	1.145
2	50	25	25	2	1.4
3	25	25	50	2	0.749
4	12.5	50	12.5	2	0.677
5	33.33	33.33	33.33	2	0.99

The samples were pressed with an 800 MPa force with a Spanish-made press equipment **Fig 4** after weighing and mixing the powder. Delaminated (cracking across the particle) Specimens were failing in the testing methods at very high pressing pressure; this is mostly because of the work-hardening effect. However, extremely low pressure was unable to produce a strong enough compact. Detailed characterization and Analyze the Elemental Composition of the FGMs compound powder was carried out using X-ray fluorescence XRF. The mixed powders were filled and uniaxially cold pressed in a steel die as shown in **Fig 2**. Pressures of compaction ranged from 50 to 800 MPa [109]. Compaction pressures ranged are used to abstain dynamic load characteristic in this research. Aluminum compaction behavior was quantified by taking into account the densification of metal particles during uniaxial compaction. The influence on samples along with their morphology was considered when evaluating compressibility behavior. The ability can analyze the effect of particle geometries and matrices stiffness on the compression test is allowed by a development of compaction values along pressing pressure.

The greens preform are weighed with 0.001 g accuracy. A micrometer caliper was used to measure the dimensions (0.01 mm). Then, utilizing the vacuum furnace and an argon environment, all of the green produced FGMs compacts samples were sintered at 600 °C. Three argon gas flow rates 6, 7, and 8 m/s were selected. The spaceman was sintered by warming, then to 400°C at a rate of 10°C/min for one hour, then to 620° C for three hours. The heating rate was less than 10 °C/min throughout the process. The heating rate was less than 10 °C/min throughout the process Figure to The heating rate was less than 10 °C/min throughout the process to avoid the melting point temperature of Al and keep the original shape. Sintering is a process that increases the strength of compressed beams. An argon gas environment furnace was used for the sintering process. Fig 3 depicts the temperature change in the furnace like a time - dependent during the sintering temperature. All zinc stearate in the sample evaporates almost completely at 335°C, and the structure is completely destroyed after sintering. During sintering, argon gas is provided at a steady flow rate of 50 ml/min to prevent aluminum from oxidizing Fig. 3. Fig. 4 depicts the final shape of the beam samples

Figure 2. A steel dies.

.

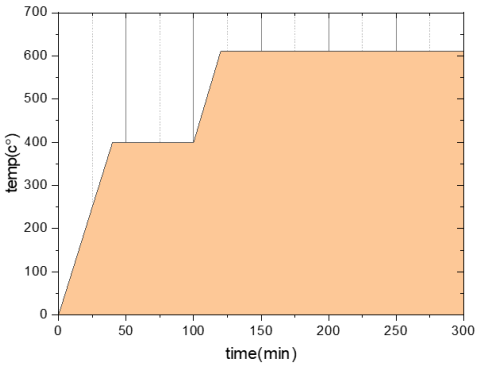

Figure 3. During the sintering process, the temperature of the furnace changes over time

Figure 4. final shape of the beam samples

3. Results and discussions

Other than Ni, Steel, and Al, the XRF gives confirmation of elements. The XRF data also serve in validating the purity and quantity of the initial elemental powders, as well as preventing contamination of the powders during mixing and sintering sample manufacturing. Detailed characterization and Analyze the Elemental Composition of the FGMs compound powder was carried out using X-ray fluorescence XRF **Table 2**.

Table 2. Chemical compositions percentage Wt. of sample 1 by using XRF test.

Layer number	Wt% Ni	Wt% Al	Wt% Fe	Wt% Mo	Wt %C	Wt% Cr
1	37.762	33.13	19..31	4.125	0.02	5.77
2	53.125	25.10	17.433	0.562	0.03	4.73
3	25.75	25.21	40.11	1.111	0.04	8.75
4	25.75	25.11	40.11	0.251	0.04	2.11
5	37.762	33.13	19..31	4.125	0.02	5.77

The mechanical behavior of Aluminum-Nickel-316steel alloy was tested experimentally according to ASTM E-8M standard. Samples were created as shown in **Fig. 5** The toughness is measured using concepts of Linear Fracture Mechanics (LEFM), as well as the structural hardness characteristics, according with ASTM E.8 standards testing protocol. Work piece tension samples with a diameter of 12.6 mm as well as a length of 3 cm in accordance with ASTM E.8M.

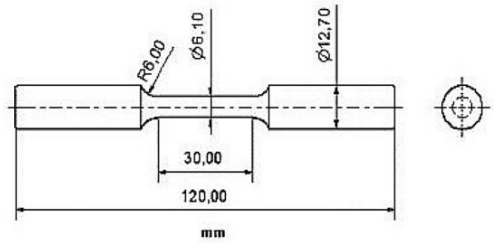

Figure 5. Tensile test specimen dimensions

The elastic modulus and as well as the maximum tensile strength of every FGM beam layer of the three samples were calculated in this manner being shown in Figures 5.4.and Figures 5.5 Elastic modulus may be seen in the graphs.

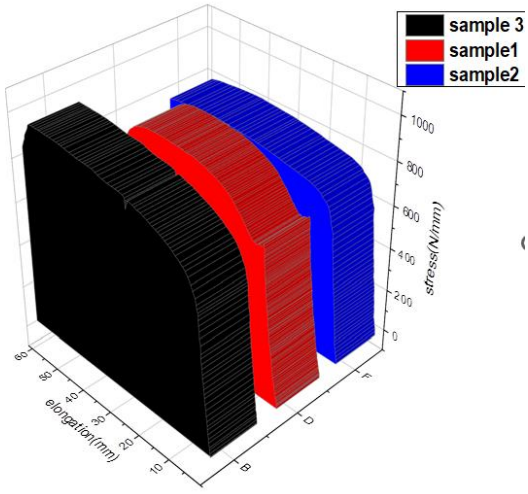

Figure 6. Values of maximum tensile strength for various Al,St,Ni ratios in 3D wall

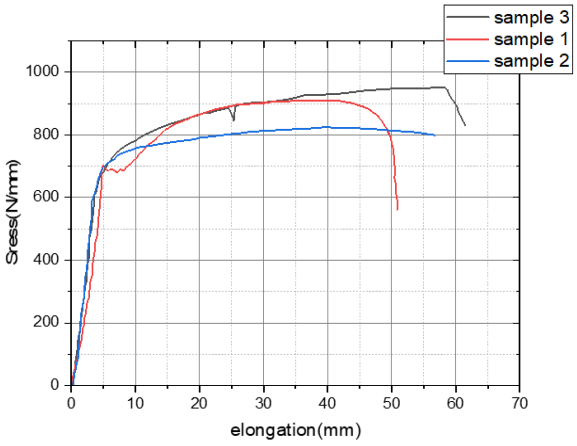

Figure 7. Values of maximum tensile strength for various Al,St,Ni ratios in 2D wall

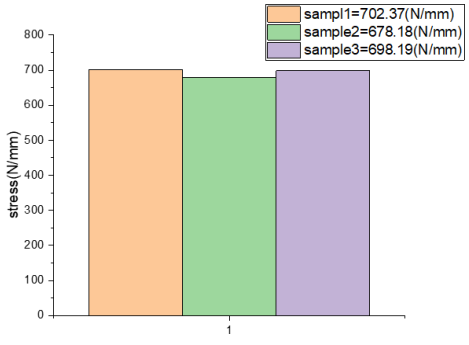

Figure 8. Yield stress comparison

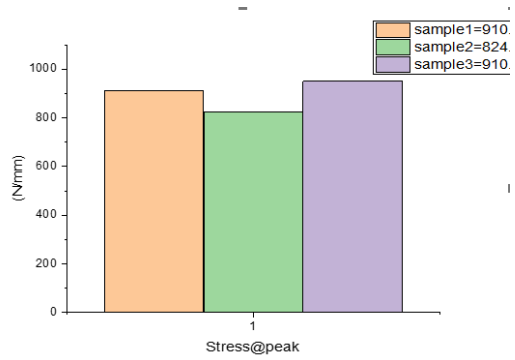

Figure 9. Stress at peak comparison

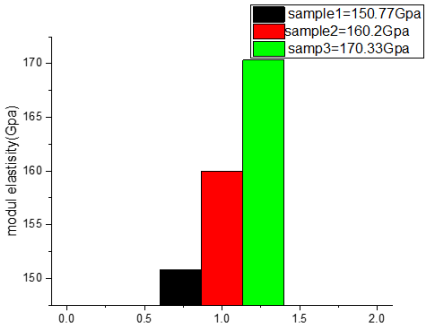

Figure 10. Elasticity modulus values for various alloy ratios (Al, Ni, Steel)

Fig. 7 demonstrate the results of tensile tests on stepwise Al/Ni/ST FGM compact specimens and each layer sample. The yield stress of an Al/Ni/Steel FGM compact specimen is shown in Figure.8 in comparison to each sample. The maximum yield stress value was found in the sample1. The yield stress and module elasticity values of Al/Ni/St FGM compact specimens are higher than those of steel (350Mpa), and this is considered a significant improvement in mechanical qualities over those of steel (100 percent steel). The ultimate stress value of Al/Ni/St FGM exceeds the ultimate stress value of stainless-steel Grade 440C(760Mpa). The Young's modulus of FGM samples is shown in Fig.10. Nickel had a Young's modulus of (211 Gpa), while aluminum had a value of (73 Gpa), and steel had a value of (200 Gpa). The three samples for the percentages of nickel-aluminum-316 Steel compact are in the range of these three values. From a thermodynamic standpoint, carbon could've been dispersed at temperatures over 730°C, but in practice, temperatures of >900°C are necessary to enable rapid and thorough dissolution. Due to the slower diffusion of metals alloy elements, even increased temperature are necessary, and involve various Ni doesn't really fully homogenize even at the greatest temperature, because of Fe's extremely slow solid phase diffusion. Steel 316L was chosen for this study because it has a low carbon content and hence avoids excessive sintering temperatures. Because the Al and SUS316L particles reacted together during the SPS process, intermetallic compounds such as Cr.Ni.Fe.Fe and AlFe3 were produced in the Al-SUS316L composite, according to the X-ray diraction (XRD) patterns. XRD and scanning electron microscopy (SEM) were also used to demonstrate the presence of these intermetallic complexes .2 deg/min for scanning. The XRD test results of layer1-sample1 are shown in the **Fig. 11** and **Table 3**.

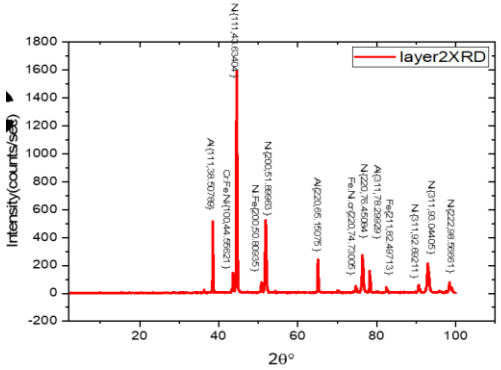

Figure .11 XRD of layer1-sample1-layer1

Table 3 XRD data of layer 2-sample 1

Hkl	Dhkl(n.m)	Peak position (2θ °)	FWHM β(°)
Al{111,38.50789}	59.16903096	38.50789	0.14854
Ni{111,43.63404 }	40.56789866	43.63404	0.22031
Cr.Fe.Ni{100,44.55621 }	37.84052244	44.55621	0.23696
Ni.Fe{200,50.80935 }	34.03970650	50.80935	0.26985
Ni{200,51.89963 }	31.86370773	51.89963	0.2896
Al{220,65.15075 }	44.89085534	65.15076	0.21934
Fe.Ni.cr{220,74.73005 }	30.85218341	74.73005	0.33838
Ni{220,76.45084 }	28.52529078	76.45084	0.37027
Al{311,78.29929 }	35.8318282	78.29929	0.2986
Fe{211,82.49713 }	31.67851215	82.49713	0.34837
Ni{311,92.69211 }	27.44187834	90.69211	0.43021
Ni{311,93.04405 }	23.02792293	93.04405	0.52366
Ni{222,98.56661 }	21.25812063	98.56661	0.59835

All of the data is calculated with the use of a panalytical X, PERT program and JCPDS (publishing and sharing powder diffraction data for material identification) or ICDD cards for XRD analysis. Equation (4-1) is used to calculate D(h,k,l) spacing, as indicated in table 4. (3,4,5,6,7). FWHM is used in XRD for calculating crystallite size by using Scherrer equation.
Fig. 12 depicts the morphologies of pure Al, Ni, and SUS316L powders. Pure aluminium powder has an uneven and rough surface with varying particle size distributions (**Fig .12a**). The SUS316L powder **(Fig .12b)** and pure nickel powder (**Fig .12c**) both displayed irregular morphologies; however, the nickel powder particles had rougher surfaces than the pure Al

and steel316L particles. Similar to the pure Al,Ni, and SUS316L powders, the Al-Ni-SUS316L composite powder of sample 1 -layered 2 **(Fig. 12d)** displayed a wide size distribution of irregular and rough-surfaced particles. The composite powder particles, on the other hand, had smoother surfaces than the SUS316L, Ni powder since the former had been crushed and blended before usage and subjected to mechanical forces during the ball milling process.

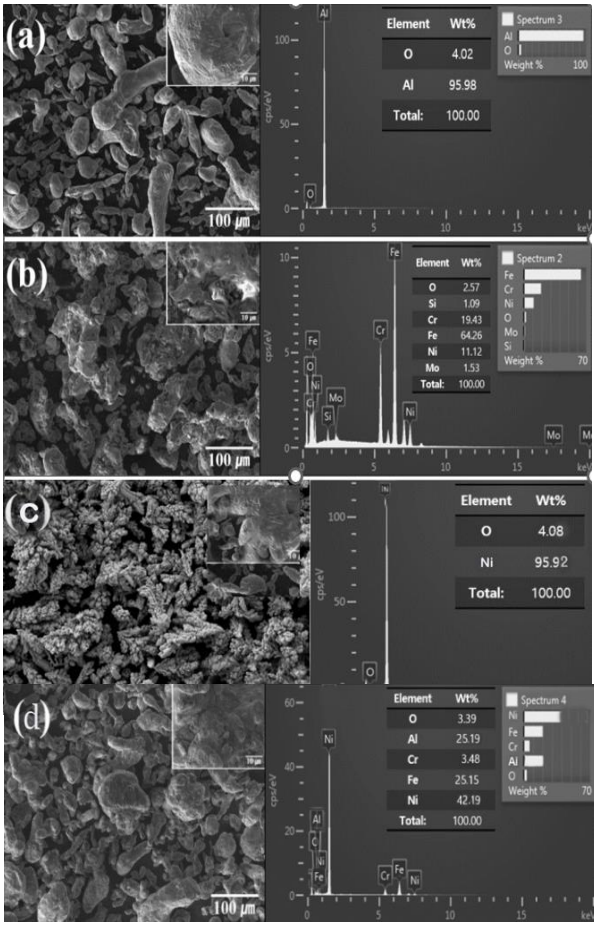

Figure 12. SEM micrographs and EDS spectra of (a) pure Al, (b) SUS316L, (c) pure Ni, and (d) Al – Steel 316L and Ni composite powder sample 1-lyered 2

The phases of the four powders, their sintered bulks, and the composite examined with XRD diffraction patterns are shown in Figure 4.12. For comparison with the composite, pure Al, Ni, and SUS316L bulk were produced under the same FGMs process parameters. Fig.13 shows the peaks for Al and -Fe alone in the Al, Ni,Steel S316L, and Al-Ni-steel 316L composite powders. This means that during the ball milling process, the Al and Steel 316L powders did not react with each other.

As illustrated in Fig.14, intermetallic compounds such as Cr.Ni. Fe111, Cr.Ni. Fe200, Al.Ni311), Cr.Ni.Fe222, and Al.Fe.Mn.Mo were discovered. The sintering technique was thought to have created these intermetallic compounds by reacting Al, Ni, and the components of SUS316L. It's further corroborated by the fact that the peaks of these intermetallic compounds were absent from the Al-Steel 316L-Ni composite's direction pattern. The contaminants and oxide coatings of the particle surfaces created during the sintering process [21,22] were removed by cleaning . Because of the high temperature of the sintering, the particles locally react with one another, potentially resulting in the creation of intermetallic compounds [23]. The sintering procedure was carried out at 630 C in this work, which is lower than the melting temperature of Al .In the semisolid state. The liquid phase did not exist indefinitely; it appeared in little amounts and then vanished. Due to the existence of micro-plasma, it appears that the temperature within the mold was over 630 C throughout the sintering process. The temperatures inside the mold and at the mold's surface may differ slightly [24]. As a result, we discovered that we couldn't process the materials above 630 degrees Celsius due to the formation of liquid phases.

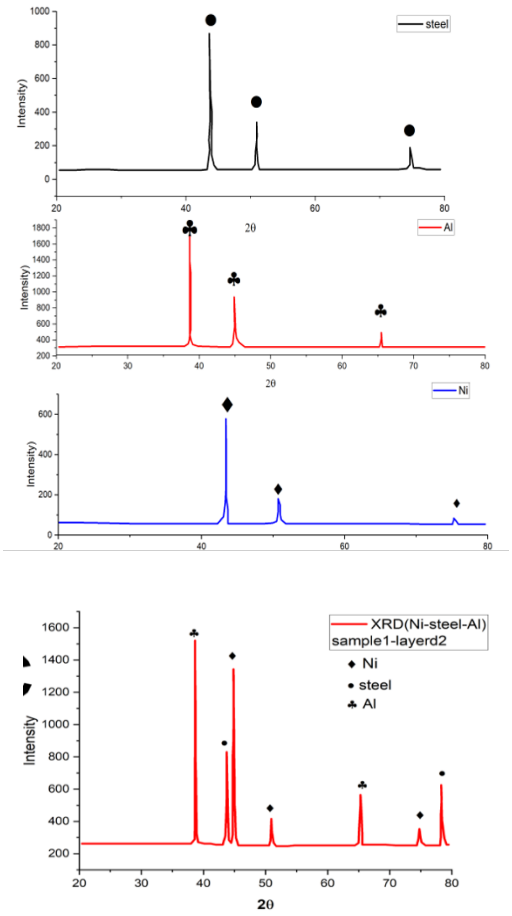

Figure.13 Pure Al, Steel316L, Ni, and Al-Ni-Steel powder XRD patterns

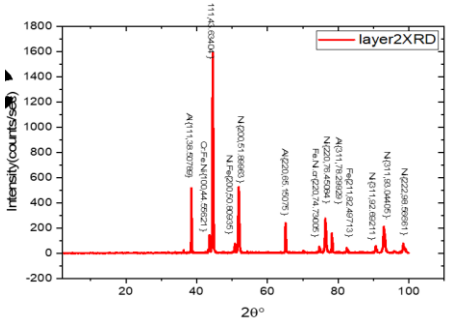

Figure.14 XRD of layer2- sample1

Fig.15 shows SEM micrographs and EDS of pure Al bulk, Steel316L bulk, Ni bulk, and Al -Steel316L-Ni composite. Because the sintering temperature was so close to the melting point of Al, this happened. Fig.15a, on the other hand, shows some grooved-holes that appear to be pores. These grooved-holes are thought to have been made by over-etching used to examine the microstructure of pure Al bulk. Because the sintering temperature is substantially lower than the melting point of Steel S316L, the Steel 316L bulk seems to have many pores and a much lower density, as shown in Fig.15b. Because ductile Al has a larger relative density table 4., the composite has a higher density. Furthermore, due to the repositioning of the particles in the semisolid state during the sintering process, densification happens quickly once the liquid phase is produced [25]. As a result, liquid phase could seep into the pores of the composite, causing it to fail.

Table 4 The physical relative density properties of Al, Ni, Steel and Al-Ni-steel composites

Sample	Relative density %
Pure Al	98.4
Pure Ni	80.9
Pure steel 316	79.9
Al-Ni-Steel316	95.8

Because the heating rate is substantially lower than the values melting point of Steel316L, the Steel bulk and Nickel seems to have numerous pores and a significantly lower density in other hands, as shown in Fig.16 and Table 4. Surprisingly, as shown in Fig.16 c, the Al-steel316L-Ni (sample 1-layered 2) composite has a high density of almost 95 percent. The liquid Al (25 percent) appears to penetrate the Al vol. Percent Steel 316L composite's pores and effectively seal them shut. In other words, the higher density of ductile Al is responsible for the higher density of the composite. Additionally, due to the repositioning of the particles in the semisolid state throughout sintering process, the densification happens quickly after the liquid phase is produced [25].

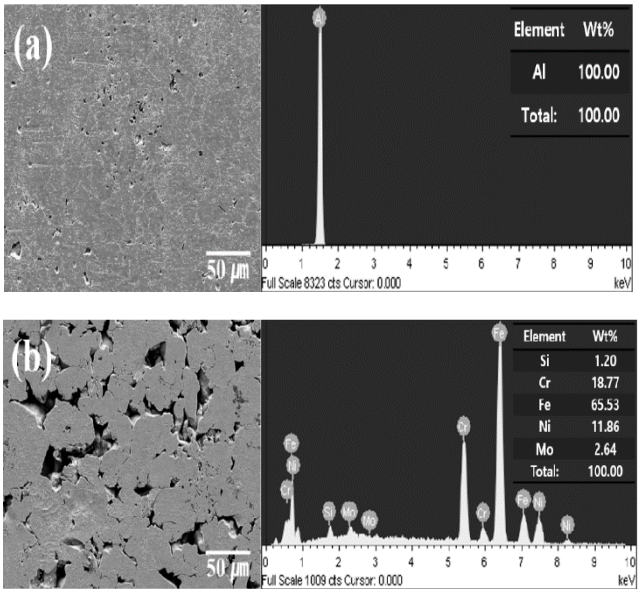

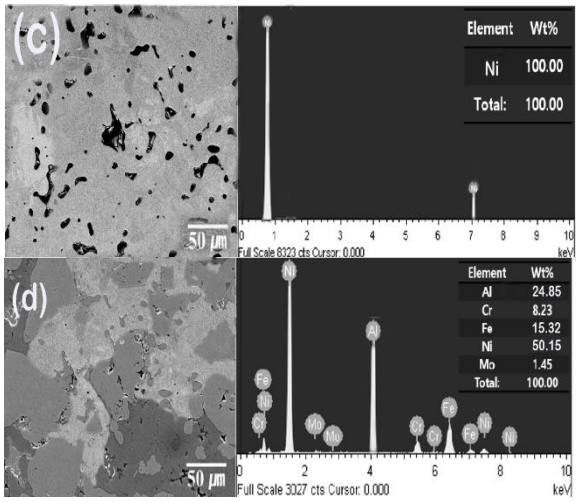

Figure 16. (A) Pure Al bulk, (B) a steel 316L bulk, (C) Pure Ni bulk and(D) composite made of 25% aluminum, 25% steel, and 25% nickel are shown in SEM micrographs and EDS analysis, respectively

The XRD patterns, SEM, and EDS all supported the existence of these intermetallic complexes. The Al-Steel316L-Ni composite's mechanical hardness may be raised as a result of the formation of these high-hardness intermetallic compounds between the Al and Steel316L matrix. Similar to this, intermetallic compounds are thought to establish a strong chemical link between the Al, Ni, and Steel 316L matrix, perhaps enhancing load transfer. Additionally, the composite could become stronger as a result of the semisolid state sintering process. As was already indicated, the increased mechanical capabilities of the composite may be due to the densifying tendency seen during the semisolid state sintering process. Because the Steel316L, Ni, Al matrix and intermetallic compounds were mixed, it's possible to increase the bond strength between the matrices.

4. Conclusions

With the aid of mechanical ball milling and semisolid state sintering, we have produced Al-SUS316L composites with success. Vickers hardness for the composite made of (percentage 50 Ni, percent 25 Al, and per cent 25 Steel316L) is about 190 HV. By combining Ni ,Al and SUS316L, intermetallic compounds like Cr.Fe.Ni and Ni.Fe were created. The Al-SUS316L composite's XRD patterns, SEM (EDS), and EDS mapping results all supported the presence of these intermetallic compounds. It's probable that the development of these intermetallic compounds with high mechanical hardness plays a significant role in the Al-SUS316L composite's strengthening mechanism. Additionally, the strengthening effect of the composite may also be influenced by the semisolid state sintering process and green pressing. To clearly identify the components impacting the mechanical strength of the composite, further thorough studies are required, such as TEM, tensile strength analyses, and corrosion resistance tests. Thus, the Al-SUS316L composite created by the cold pressing and sintering process might be used in the engineering industry as a lightweight, high-hardness multifunctional composite material.

REFERENCES

[1] R. Singh, V. Bhavar, P. Kattire, S. Thakare, S. Patil, and R. K. P. Singh, "A Review on Functionally Gradient Materials (FGMs) and Their Applications," *IOP Conference Series: Materials Science and Engineering*, vol. 229, no. 1, Sep. 2017, doi: 10.1088/1757-899X/229/1/012021.

[2] "(PDF) Dental implants from functionally graded materials | Nahrizul Kadri and M. Mehrali - Academia.edu." https://www.academia.edu/14248793/Dental_implants_from_functionally_graded_materials (accessed Jul. 08, 2022).

[3] M. Dogan, "Delamination failure of steel single angle sections," *Engineering Failure Analysis*, vol. 18, no. 7, pp. 1800–1807, Oct. 2011, doi: 10.1016/J.ENGFAILANAL.2011.04.009.

[4] B. L. Bramfitt and A. R. Marder, "A study of the delamination behavior of a very low-carbon steel," *Metallurgical Transactions A 1977 8:8*, vol. 8, no. 8, pp. 1263–1273, 1977, doi: 10.1007/BF02643841.

[5] P. T. Thang and J. Lee, "Free vibration characteristics of sigmoid-functionally graded plates reinforced by longitudinal and transversal stiffeners," *Ocean Engineering*, vol. 148, pp. 53–61, Jan. 2018, doi: 10.1016/J.OCEANENG.2017.11.023.

[6] E. Bódis, M. Jakab, K. Bán, and Z. Károly, "Functionally Graded Al2O3–CTZ Ceramics Fabricated by Spark Plasma Sintering," *Materials 2022, Vol. 15, Page 1860*, vol. 15, no. 5, p. 1860, Mar. 2022, doi: 10.3390/MA15051860.

[7] A. Canakci, T. Varol, F. Erdemir, S. Ozkaya, and H. Mindivan, "Microstructure and properties of Fe-Al intermetallic coatings on the low carbon steel synthesized by mechanical alloying," *International Journal of Advanced Manufacturing Technology*, vol. 73, no. 5–8, pp. 849–858, 2014, doi: 10.1007/S00170-014-5851-2.

[8] J. Matějíček, J. Antoš, and P. Rohan, "W + Cu and W + Ni Composites and FGMs Prepared by Plasma Transferred Arc Cladding," *Materials 2021, Vol. 14, Page 789*, vol. 14, no. 4, p. 789, Feb. 2021, doi: 10.3390/MA14040789.

[9] K. B. Panda and K. S. Ravi Chandran, "Titanium-titanium boride (Ti-TiB) functionally graded materials through reaction sintering: Synthesis, microstructure, and properties,"

[10] *Metallurgical and Materials Transactions A 2003 34:9*, vol. 34, no. 9, pp.

[11] I. M. El-Galy, M. H. Ahmed, and B. I. Bassiouny, "Characterization of functionally graded Al-SiCp metal matrix 1993–2003, 2003, doi: 10.1007/S11661-003-0164-3.

[12] composites manufactured by centrifugal casting," *Alexandria Engineering Journal*, vol. 56, no. 4, pp. 371–381, Dec. 2017, doi: 10.1016/J.AEJ.2017.03.009.

[13] J. F. Groves and H. N. G. Wadley, "Functionally graded materials synthesis via low vacuum directed vapor deposition," *Composites Part B: Engineering*, vol. 28, no. 1–2, pp. 57–69, Jan. 1997, doi: 10.1016/S1359-8368(96)00023-6.

[14] Z. qiang Tan, Q. Zhang, X. yi Guo, W. jiang Zhao, C. shang Zhou, and Y. Liu, "New development of powder metallurgy in automotive industry," *Journal of Central South University 2020 27:6*, vol. 27, no. 6, pp. 1611–1623, Jul. 2020, doi: 10.1007/S11771-020-4394-Y.

[15] S. Hameed Al-Shafaie, N. S. Radhi, and M. Aziz Hussein, "Preparation and Investigation Mechanical Properties of Functionally Graded Materials of Aluminum-Nickel Alloys," *Journal of Mechanical Engineering Research and Developments*, vol. 44, no. 4, pp. 102–109.

[16] M. R. SITI NUR HAZWANI, L. X. LIM, Z. LOCKMAN, and H. ZUHAILAWATI, "Fabrication of titanium-based alloys with bioactive surface oxide layer as biomedical implants: Opportunity and challenges," *Transactions of Nonferrous Metals Society of China*, vol. 32, no. 1, pp. 1–44, Jan. 2022, doi: 10.1016/S1003-6326(21)65776-X.